AGU PUBLICATIONS

JGR

Journal of Geophysical Research: Earth Surface

RESEARCH ARTICLE
10.1002/2017JF004354

Key Points:
- Data collected from an active drumlin field guide the formulation of a new mathematical model of drumlin formation
- Sediment transport feedbacks in the model cause subglacial topographic perturbations to migrate downglacier and grow at an increasing rate
- Net aggradation or erosion can accompany drumlin growth, and drumlin heights and stratigraphy generally correspond with observations

Correspondence to:
N. R. Iverson,
niverson@iastate.edu

Citation:
Iverson, N. R., McCracken, R. G., Zoet, L. K., Benediktsson, Í. Ö., Schomacker, A., Johnson, M. D., & Woodard, J. (2017). A theoretical model of drumlin formation based on observations at Múlajökull, Iceland. *Journal of Geophysical Research: Earth Surface*, *122*, 2302–2323. https://doi.org/10.1002/2017JF004354

Received 9 MAY 2017
Accepted 13 NOV 2017
Accepted article online 20 NOV 2017
Published online 6 DEC 2017

A Theoretical Model of Drumlin Formation Based on Observations at Múlajökull, Iceland

N. R. Iverson[1], R. G. McCracken[1], L. K. Zoet[1,2], Í. Ö. Benediktsson[3], A. Schomacker[4], M. D. Johnson[5], and J. Woodard[2]

[1]Department of Geological and Atmospheric Sciences, Iowa State University, Ames, IA, USA, [2]Department of Geoscience, University of Wisconsin—Madison, Madison, WI, USA, [3]Institute of Earth Sciences, University of Iceland, Reykjavík, Iceland, [4]Department of Geosciences, UiT—The Arctic University of Norway, Tromsø, Norway, [5]Department of Earth Sciences, University of Gothenburg, Göteborg, Sweden

Abstract The drumlin field at the surge-type glacier, Múlajökull, provides an unusual opportunity to build a model of drumlin formation based on field observations in a modern drumlin-forming environment. These observations indicate that surges deposit till layers that drape the glacier forefield, conform to drumlin surfaces, and are deposited in shear. Observations also indicate that erosion helps create drumlin relief, effective stresses in subglacial till are highest between drumlins, and during quiescent flow, crevasses on the glacier surface overlie drumlins while subglacial channels occupy intervening swales. In the model, we consider gentle undulations on the bed bounded by subglacial channels at low water pressure. During quiescent flow, slip of temperate ice across these undulations and basal water flow toward bounding channels create an effective stress distribution that maximizes till entrainment in ice on the heads and flanks of drumlins. Crevasses amplify this effect but are not necessary for it. During surges, effective stresses are uniformly low, and the bed shears pervasively. Vigorous basal melting during surges releases debris from ice and deposits it on the bed, with deposition augmented by transport in the deforming bed. As surge cycles progress, drumlins migrate downglacier and grow at increasing rates, due to positive feedbacks that depend on drumlin height. Drumlin growth can be accompanied by either net aggradation or erosion of the bed, and drumlin heights and stratigraphy generally correspond with observations. This model highlights that drumlin growth can reflect instabilities other than those of bed shear instability models, which require heuristic till transport assumptions.

1. Introduction

Conceptual and mathematical models of drumlin formation have different origins. Conceptual models tend to be derived from field observations from a particular locality or set of localities (e.g., Eyles et al., 2016; Menzies et al., 2016). The large number of such models likely reflects the diversity of the internal characteristics of drumlins (e.g., Stokes et al., 2011, 2013) and the roominess of interpretations that the incomplete geologic record allows. In contrast, in mathematical models of drumlin formation, which are fewer, the starting point is not a specific set of field observations. For example, in the largest family of such models, relationships are posited between basal shear stress, normal stress on the bed, and sediment transport that are designed to produce local longitudinal gradients in till flux in a deforming bed that create a ridge-forming instability (Fowler, 2000, 2009, 2010; Hindmarsh, 1998; Schoof, 2007; Stokes et al., 2013). Sediment transport by subglacial water flow can be added to this bed-shear instability so that drumlin-like hills, rather than transverse ridges, result (Fannon et al., 2017; Fowler & Chapwanya, 2014). A primary goal of these models and less physically based quantitative models (Barchyn et al., 2016) is to reproduce observed patterns of drumlins and other subglacial bedforms.

If there are indeed some underlying processes common to the formation of all drumlins—an appealing (e.g., Clark, 2010) but not necessarily correct proposition (Möller et al., 2016)—then neither approach is ideal. Conceptual models, that is, qualitative hypotheses, are not subject to the binding and illuminating physical rules that mathematical formalization requires and do not provide quantitative benchmarks for testing. On the other hand, mathematical models that are not tied to field observations and known material behavior risk being physically irrelevant.

With this study, we make use of a set of observations at Múlajökull, Iceland—a receding surge-type glacier that has built and exposed a field of 143 drumlins (Figure 1)—to develop a rudimentary quantitative

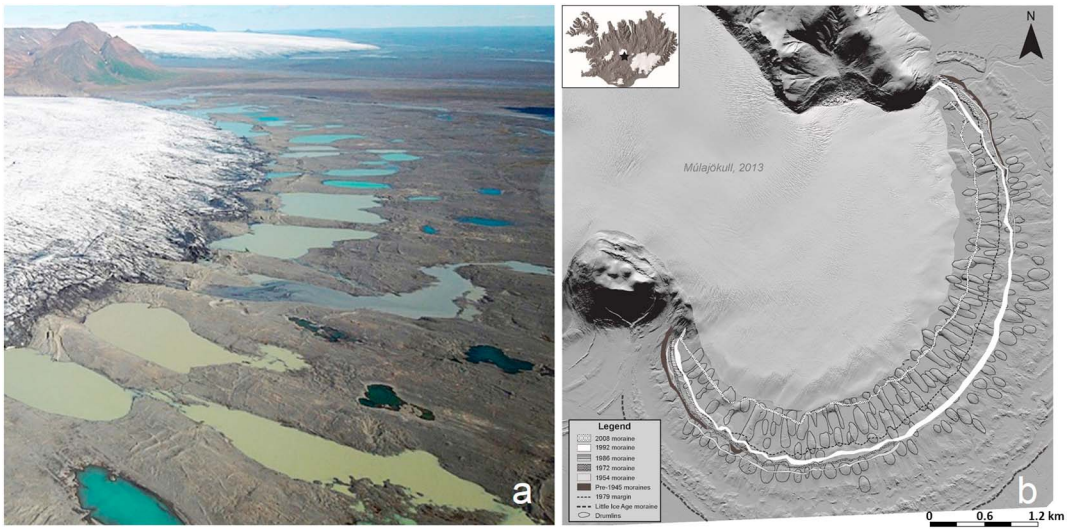

Figure 1. (a) Oblique view of the Múlajökull drumlin field, looking north. (b) LiDAR hillshade map of Múlajökull and its forefield from 2013, with ice indicated by light shading and drumlins outlined in black. Moraines associated with surges, as mapped by Jónsson et al. (2014) and Sigurkarlsson (2015), are also shown, including the Little Ice Age moraine (heavy dashed black line; modified from McCracken et al., 2016).

model of their formation. Patterns of basal till movement and effective stress on the bed within and between drumlins are provided by, respectively, 2,200 measurements of till anisotropy of magnetic susceptibility (AMS) calibrated to laboratory ring shear experiments and a similar number of till-density measurements calibrated to laboratory consolidation tests (McCracken et al., 2016). Additional guidance and constraints are provided by stratigraphic observations (Benediktsson et al., 2016; Johnson et al., 2010), observations and analyses of drumlin shape (Benediktsson et al., 2016; Jónsson et al., 2014) and forefield elevation (McCracken et al., 2016), ground-penetrating radar data that bear on drumlin structure, and baseline glaciological data from Múlajökull (Björnsson et al., 2003; Minchew et al., 2016).

These constraints motivate a model in which sediment transport feedbacks cause gentle topographic perturbations on the bed to grow into drumlins through multiple surge cycles. The model illustrates how different sediment transport mechanisms than those of the bed shear instability model could result in feedbacks that form drumlins. The new model also highlights physical underpinnings that the two models share. It is the first quantitative model of drumlin formation derived from the field observations at Múlajökull.

2. Observations at Múlajökull

The piedmont, warm-based glacier, Múlajökull, an outlet glacier of the Hofsjökull ice cap, has surged eight times since 1924, with quiescence periods of 5–30 years (Björnsson et al., 2003). Evidence of earlier surges in the form of multiple end moraines is ubiquitous, including the glaciotectonic Little Ice Age terminal moraine that formed between 1717 and 1760 (Benediktsson et al., 2016; Jónsson et al., 2014). Most of the recent surges have resulted in glacier advances of 200–400 m, each leaving end moraines (Figure 1b; Benediktsson et al., 2015; Johnson et al., 2010). The most recent surge in 2008 caused only a ~20 m advance but left a prominent glaciotectonic moraine (Benediktsson et al., 2016). The last major surge in 1992 terminated at approximately the same position as the three previous surges in 1954, 1972, and 1986 (Jónsson et al., 2014). Durations of surges are poorly known but do not seem to have exceeded 2 years (Björnsson et al., 2003). Ice velocities during surges are unknown. Repeated surveys of ice movement within 500 m of the margin in 2009–2015 indicated speeds of ~7–15 m/a during the current period of quiescent flow.

The drumlins occur in an arc-shaped zone within ~1.2 km of the glacier margin (Figure 1). More drumlins continue to be exposed as the margin recedes (Benediktsson et al., 2016; Johnson et al., 2010; Jónsson et al., 2014), and ground penetrating radar reveals that drumlins extend upglacier from the margin several hundred meters (Lamsters et al., 2016). Exposed drumlins were shaped by ice no farther than ~2 km from the former glacier margin at its maximum, as indicated by the position of the Little Ice Age terminal moraine (Figure 1b;

e.g., Benediktsson et al., 2015; Jónsson et al., 2014). Most drumlins are 100–400 m in length, 50–150 m in width, and 2–14 m in height with swales between them commonly occupied by lakes that reduce the apparent dimensions of the drumlins (Benediktsson et al., 2016). These dimensions fall within the lower range observed in Pleistocene drumlin fields (Clark et al., 2009). Mean elongation ratios of drumlins are larger upglacier from the end-moraine complex that marks the extents of the 1954–1992 surges (3.0), than they are downglacier from it (1.9), consistent with drumlin streamlining increasing with successive surge cycles (Benediktsson et al., 2016).

Stratigraphic observations indicate that the drumlins consist primarily of basal till units deposited during surges but that erosion has occurred along drumlin flanks and heads, contributing to their relief (Johnson et al., 2010). The 2008 surge left a distinctive basal till that drapes drumlins and interdrumlin areas everywhere upglacier from the 2008 surge moraine (Benediktsson et al., 2016). Moreover, an older uppermost till at two exposures downglacier from the 2008 moraine can be traced in stream cuts to the 1992 surge's end moraine but not beyond it (Johnson et al., 2010), indicating that the till was deposited by the 1992 surge. Stratigraphic observations also indicate, however, that the uppermost till in most exposures rests unconformably on older tills both along drumlin sides (Benediktsson et al., 2016; Johnson et al., 2010) and at the head of the only drumlin with a good longitudinal stratigraphic section (Benediktsson et al., 2016). Time series of ice-margin fluctuations (Benediktsson et al., 2016, their Figure 1B) show that parts of these sections with unconformities were not exposed subaerially between surges before ~10 years ago, indicating that the erosion occurred subglacially. Similar unconformities, including additional ones at drumlin heads, have been identified in multiple drumlins with ground-penetrating radar (Woodard, 2017; Figure 2).

Till fabrics (81) based on orientations of principal magnetic susceptibilities from eight drumlins and three intervening areas, together with ancillary clast fabric data, indicate that till was deposited during shear deformation, with shear azimuths that diverge and converge about drumlin long axes and shear planes that conform to drumlin topography (McCracken et al., 2016). These data are consistent with observations of till layers dipping in the directions of local drumlin slopes (Benediktsson et al., 2016). AMS fabrics from interdrumlin areas indicate purely downglacier flow, parallel to long axes of adjacent drumlins, with shear planes dipping mildly downglacier (McCracken et al., 2016), consistent with till layers that dip similarly in such areas (Benediktsson et al., 2016). These observations collectively indicate that till deposition during surges occurred on drumlins, ruling out the possibility that deposition occurred prior to drumlinization. Importantly, owing to shear deformation near the bed surface that accompanies till lodgment (Boulton et al., 1974; Larsen et al., 2004; Piotrowski et al., 2004; Tulaczyk, 1999), AMS fabrics cannot be used to distinguish till transported in ice from till transported in a deforming bed (Iverson et al., 2008).

Other data reinforce that although erosion helped produce drumlin relief, the process was accompanied by net aggradation of the forefield (McCracken et al., 2016). Topographic profiles indicate that proglacial sediments thin abruptly outside the moraine complex that marks the extents of the 1954–1992 surges (Figure 1b). Thicker sediment inside the proximal zone subject to the most surges indicates that surging and drumlin formation were accompanied by net thickening of proglacial sediments (McCracken et al., 2016).

AMS fabric patterns indicative of strain dominated by longitudinal compression and vertical extension—as measured, for example, in moraines subjected to such strain (Ankerstjerne et al., 2015)—are absent in till both within and between drumlins (McCracken et al., 2016). Rather, fabric patterns indicate strain dominated by simple shear.

More than 2,000 measurements of till density indicate that till within drumlins was systematically less dense than till between drumlins (McCracken et al., 2016). Laboratory calibration of till density to effective stress shows that the maximum effective stress on the till bed since its deposition was on average ~100 kPa higher between drumlins than within them, despite the tendency for the glacier surface to be lower over interdrumlin areas. This pattern of till density was set during quiescent periods between surges, when subglacial water flow was channelized, and basal water pressure was lower than during surges (e.g., Kamb et al., 1985), maximizing effective stress on the bed and till consolidation.

No measurements at Múlajökull bear directly on its subglacial hydrology, but some observations are suggestive. During the glacier's current quiescent phase, water emerges from the margin through portals that tend to be in low areas between drumlins (McCracken et al., 2016), and the one esker in the forefield occupies such a swale. In agreement with these observations, channel cuts high on drumlin surfaces are rare, accounting for

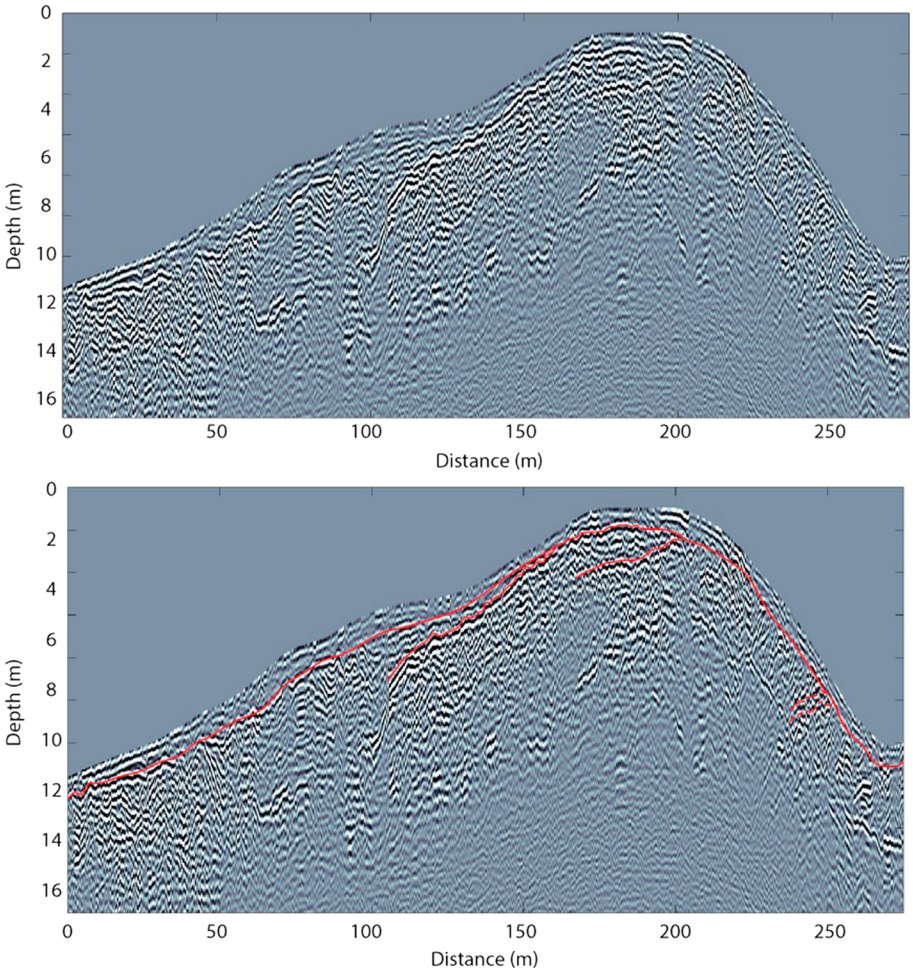

Figure 2. Longitudinal section through a drumlin at Múlajökull, as indicated by ground-penetrating radar (GPR) data gathered in 2013 with a 200 MHz antenna, revealing an unconformity at the drumlin head and sediment layers that dip downglacier (modified from Woodard, 2017). Glacier flow was from right to left. The velocity used for migration and depth conversion was 0.0825 m/ns. Red lines indicate stratigraphic layers correlated to other GPR transects.

the limited number of stratigraphic exposures within drumlins (Benediktsson et al., 2016; Johnson et al., 2010). These observations indicate that during quiescent periods, water generally flowed in channels that occupied low areas between drumlins—a reasonable expectation for a thin, gently sloping, post-surge ice margin (Shreve, 1972). This conclusion agrees with the pattern of effective stress indicated by till densities, given that water pressure in such channels should be low compared to that of interfluve areas. Clastic dikes, which cut through till in some drumlins and indicate preferred pathways for water flow when the drumlins were subglacial, dip away from drumlin long axes and toward interdrumlin areas (Benediktsson et al., 2016, their Figure 9), consistent with channels in such areas carrying water at lower hydraulic potential than in interfluve areas.

A final observation is that drumlins beneath the outermost ~500 m of the glacier, where the ice is less than ~100 m thick (Lamsters et al., 2016; Minchew et al., 2016), are coincident with overlying crevasse swarms (Johnson et al., 2010). This observation applies to the glacier as photographed in 1995 after the 1992 surge (Johnson et al., 2010), as well as to the margin more recently (Benediktsson et al., 2016; Johnson et al., 2010).

3. Rationale for Model Formulation

Any drumlin model applicable at Múlajökull must include the effects of till deposition and erosion and of multiple surge cycles. Although compelling evidence indicates that deposition occurs during surges, the timing

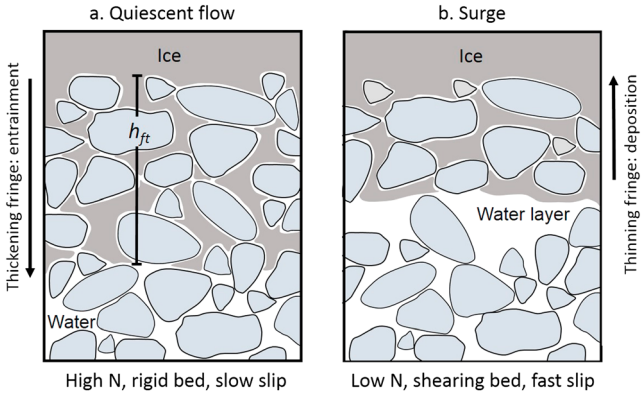

Figure 3. Frozen fringe of Rempel (2008), with interconnected water films along particles, during (a) quiescent flow when ice is in intimate contact with the till bed across thin water films, allowing regelation infiltration, fringe growth to thickness, h_{ft}, and sediment entrainment from the bed; and during (b) surging when ice is separated from the bed by a discontinuous layer of through-flowing water. The water layer prevents regelation infiltration, so frictional dissipation of heat in the deforming bed melts the fringe, releases debris from ice, and deposits till on the bed by lodgment.

of erosion that helps carve drumlins is uncertain. A possibility is that during a given surge, deposition and erosion alternate (Johnson et al., 2010), either in space simultaneously or in time such that, for example, deposition follows local erosion as the surge progresses. However, there is no field evidence or obvious rationale for asserting heterogeneity in space or time at the scales of drumlins during the surge phase, remembering that measured till densities reflect consolidation during higher effective stresses associated with quiescent flow rather than surging flow. The distributed state of the subglacial hydraulic system and the resultant uniformly low effective stress on the bed expected during surges indicate that the soft bed over drumlin length scales should be more or less uniformly weak. This conclusion follows from considering the till to be a Coulomb (i.e., frictional) plastic with its strength set by the effective stress (Cuffey & Paterson, 2010). Thus, a null hypothesis is that the soft bed was subject to uniform deformation during surges, without the heterogeneous till deformation that could cause local flux divergence (here and elsewhere we use the term to refer to till flux imbalances resulting only from bed shear) and generation of relief. This hypothesis is consistent with the basal till layer of approximately uniform thickness deposited both on and between drumlins by the most recent (2008) surge (Benediktsson et al., 2016) and with the lack of AMS fabric evidence for longitudinal compression or extension that would accompany flux divergence in a shearing bed.

We instead explore the idea that nonuniform erosion of the till bed occurred during quiescent periods, driven by spatial gradients in effective stress, as supported by field observations. Effective stress on the bed would have been highest near channels that occupied low areas between drumlins and lowest within drumlins, where hydraulic potential must have been sufficiently large to drive water along and through the till bed toward channels. Low effective stress on drumlins would have been reduced further by overlying crevasses in the thin glacier margin that decreased total normal stresses on the bed. Thus, unlike the case during surges, compelling evidence for effective stress gradients during quiescent flow motivates consideration of nonuniform erosion and resultant drumlin growth during periods between surges.

How might high effective stresses between incipient drumlins have caused erosion during quiescent flow? Erosive spatial gradients in till flux in a deforming bed could depend on effective stress, but during quiescent flow—particularly near the margin where drumlins have formed—the bed is unlikely to deform. Consideration of the Coulomb strength (e.g., Clarke, 2005) of the Múlajökull till, which has a high peak friction angle of 35° and a cohesion of 18 kPa (McCracken, 2015), indicates that for the basal shear stress calculated within 1 km of Múlajökull's margin (~50 kPa, Minchew et al., 2016), effective stress on the bed would need to be less than ~54 kPa to enable till yielding in shear. This value indicates, for example, that for ice 100 m thick near the margin, the pore water pressure equivalent to 85 m of head (very close to that required for complete flotation) would be necessary for till yielding. Such high values of water pressure, although they would be unsurprising during surging when the hydraulic system is distributed, are not generally expected during quiescence when water flows in channels at relatively low pressure (Cuffey & Paterson, 2010; Kamb et al., 1985), except during highly transient periods of intense melting or rainfall, which this model cannot hope to capture. Thus, most of the bed near the margin will not generally shear during quiescent flow. Indeed, the transition from a mostly rigid bed during quiescent flow to a shearing bed likely accompanies the transition to the surging state (Clarke et al., 1984).

An alternative is that water flow in channels in zones between incipient drumlins is responsible for erosion there. Although relatively low water pressure in such channels is likely responsible for the measured distribution of effective stress, the role of fluvial sediment transport is difficult to assess. Whether it results in erosion or aggradation depends on unknown spatial gradients in water discharge and sediment supply within channels.

A third hypothesis for sediment transport during quiescent flow, which we adopt, is that basal ice entrains debris by regelation infiltration (e.g., Clarke, 2005)—the process whereby ice freezes in the pore spaces of

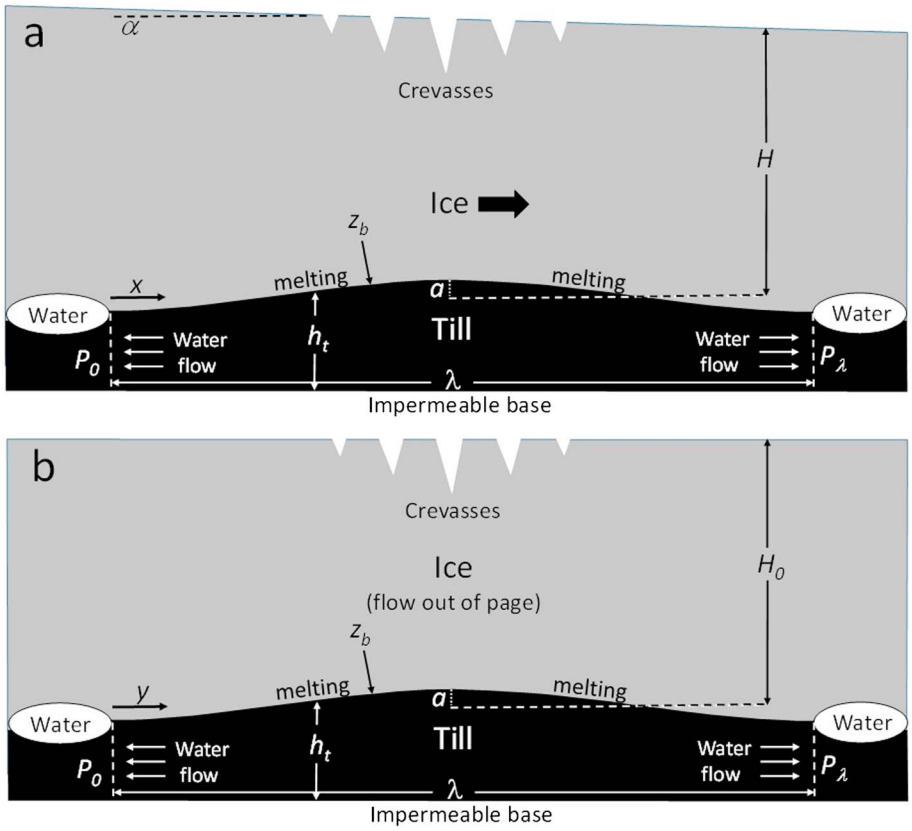

Figure 4. (a) Longitudinal view of a bed undulation during quiescent flow and bounded by channels running at water pressures P_0 and P_λ. Other parameters are defined in the text. (b). Transverse section through a bed undulation. In this case, there is no ice surface slope and $P_0 = P_\lambda$. Bed features are greatly exaggerated relative to the ice thickness.

the surface of a soft bed and entrains debris in the glacier's sole (Rempel, 2008; Figure 3a). Depths of infiltration and hence sediment entrainment are linearly proportional to effective stress on the bed in excess of a threshold value (Rempel, 2008, 2009), and infiltration is expected even if basal ice is temperate. This process has been studied in laboratory experiments with till (Iverson & Semmens, 1995) and observed beneath a temperate glacier (Iverson et al., 2007). The process is most effective in sandy, silty tills that lack significant clay (Rempel, 2008), such as those at Múlajökull (McCracken et al., 2016). Quiescent flow favors regelation infiltration because most of the glacier sole at such times will be in intimate contact with the bed across thin melt films, a requirement for the process.

In contrast, during surges, the distributed high-pressure hydrologic system will cause greater separation between ice and the glacier sole, with a discontinuous layer of through-flowing water there and lower effective stresses (Figure 3b). These factors will likely inhibit the Rempel (2008) entrainment mechanism (Creyts & Schoof, 2009). Rather, during surges, high basal slip velocities will promote heat dissipation and melting that releases debris from ice onto the deforming bed (Figure 3b).

4. Conceptual Model

During quiescent flow, gentle topographic undulations on a till bed are bounded by channels (Figure 4). Although not included in the model, the distribution of moulins observed near the margin likely helps control the spacing of these channels, and sediment transport within them could be responsible for the initial relief of undulations. Temperate ice slides across these undulations, which behave rigidly creating a flow-parallel gradient in total normal stress across them. This gradient is modified by crevasses that form above undulations to an extent that scales with ratio of their amplitude to the ice thickness. Meltwater at the bed, produced by heat dissipated by sliding and geothermal heat, flows toward bounding channels at low water pressure

(Figure 4). The likely larger discharge of water from surface melt is assumed to feed the bounding channels from the glacier surface through moulins. The pattern of basal water pressure required to drive the basally derived meltwater discharge through the till bed and the pattern of total normal stress on the bed define the steady, spatial distribution of effective stress. It modulates the thickness of debris entrained in basal ice (Figure 3a), which varies spatially and controls the evolution of relief.

During surging, the bed shears uniformly at its Coulomb strength, owing to the inefficient, distributed subglacial water system that results in low effective stress on the bed. Channels that persisted during quiescent flow are destroyed. Debris entrained in ice during quiescence is advected rapidly downglacier. Some of this debris is released from basal ice during the surge (Figure 3b) at a rate that depends on vigorous frictional heat production in the shearing bed, causing deposition of basal till on the shearing substrate. This deposition would be facilitated by release of sand and finer debris into the water layer at the bed surface (Figure 3b), with coarser debris particles being pressed into the weak yielding till (e.g., Brown et al., 1987). Additional thickening (or thinning) of the bed may be driven by downglacier changes in the flux of deforming till. Deposition ends when the surge ends, and the subglacial hydrologic system reverts back to an efficient system of channels that again bound topographic undulations. Surge cycles, therefore, cause alternating periods of spatially variable till erosion during quiescent flow and deposition of till layers during surges.

5. Model Development

5.1. Quiescent Flow

The first goal is to estimate relative depths of erosion across the bed surface during quiescent flow by determining the distribution of effective normal stress. To benefit from the transparency of analytical treatments and avoid computing numerically the three-dimensional flow of ice near the bed, we consider growth of undulations in profiles that are both parallel (*xz* plane) and perpendicular (*yz* plane) to flow but do not couple calculations in the two directions.

5.1.1. Effective Stress: Total Stresses

The horizontal till bed has topographic undulations of the form

$$z_b(x) = -a \cos\left(\frac{2\pi x}{\lambda}\right), \tag{1}$$

where x is in the direction of glacier flow, a is the amplitude, and λ is the wavelength (Figure 4a). Temperate ice of thickness $H(x)$ above the mean bed elevation and of uniform slope, α, rests on the bed. As noted, during quiescence, bed deformation beneath the glacier margin where drumlins form is unlikely, so basal slip occurs by sliding of ice across the undulations.

To determine effective normal stresses required to estimate relative depths of bed erosion, the spatial variation in total normal stress on the bed that arises due to sliding at a speed u is needed. For the case of ice with a power law rheology and no ice separation from the lee of undulations, the normal stress deviation from hydrostatic pressure on the bed due to sliding, σ_s, was estimated by Lliboutry, (1979, equation (84)) as

$$\sigma_s(x) = A' u^{1/n} \sin\left(\frac{2\pi x}{\lambda}\right), \tag{2}$$

where n is the stress exponent in Glen's flow rule (Cuffey & Paterson, 2010) and A' is a parameter that depends on the effective viscosity of the ice and the bed geometry:

$$A' = \left(\frac{1}{A}\right)^{1/n} \exp\left(\frac{n-1}{n}\right) \left[a\left(\frac{2\pi}{\lambda}\right)^2\right]^{1/n}. \tag{3}$$

A is the prefactor in Glen's flow rule, noting that it is half the value of Lliboutry's (1979) analogous parameter, B. Approximations (2) and (3) arise from using the maximum shear strain rate during sliding to define a velocity-dependent viscosity that is used in the normal stress relationship for linearly viscous ice. Appropriate for drumlin-scale undulations, regelation is neglected. Also, friction at the bed surface is neglected. In the absence of a straightforward way to include friction, we use equations (2) and (3), acknowledging that to some extent local friction at the glacier sole reduces the degree of overpressuring and underpressuring on stoss and lee surfaces, respectively.

Unequivocal evidence indicates that crevasse swarms tend to localize over drumlins at Múlajökull, so the effect of these crevasses on reducing the depth-averaged density of the ice needs to be included in considering the distribution of total normal stress on the bed (Figure 4a). We assume that the normal stress deviation from crevasse swarms, σ_c, is greatest above the peaks of undulations and mimics their form:

$$\sigma_c(x) = \rho g H(x) \phi_c \left[\cos\left(\frac{2\pi x}{\lambda}\right) - 1 \right], \tag{4}$$

where ρ is the ice density, g is the gravitational acceleration, and ϕ_c is the maximum depth-averaged porosity caused by crevasses and located above the tops of undulations. We make this idealization because although porosity from crevasses may not necessarily be symmetric about bed undulations, observations of crevasses relative to underlying drumlins provide no evidence of systematic asymmetry (e.g., Johnson et al., 2010). Crevasse volume is expected to increase with a/H_0, where H_0 is the mean of $H(x)$ across a given undulation. In the absence of definitive guidance otherwise, a linear relationship is considered:

$$\phi_c = k_c \left(\frac{a}{H_0}\right), \tag{5}$$

where k_c is a scaling parameter.

Adding the right-hand sides of equations (2) and (4) to the total normal stress on the bed due to only $H(x)$ and the bed topography yields the total normal stress on the bed, $\sigma_t(x)$:

$$\sigma_t(x) = \rho g \left\{ H(x) + a \cos\left(\frac{2\pi x}{\lambda}\right) + H(x)\phi_c \left[\cos\left(\frac{2\pi x}{\lambda}\right) - 1 \right] \right\} + A' u^{1/n} \sin\left(\frac{2\pi x}{\lambda}\right). \tag{6}$$

The first and second terms on the right-hand side describe, respectively, normal stresses from the static load of the ice and dynamic normal stresses from sliding.

Now consider a topographic perturbation of the same form as equation (1) but in the y (transverse) direction (Figure 4b). Using the same pattern of normal stress reduction due to crevasses as in the longitudinal case and noting the absence of stress variation due to sliding, provides, through modification of equation (6), the total normal stress on the bed, $\sigma_t(y)$:

$$\sigma_t(y) = \rho g \left\{ H_0 - a \cos\left(\frac{2\pi y}{\lambda}\right) + H_0 \phi_c \left[\cos\left(\frac{2\pi y}{\lambda}\right) - 1 \right] \right\}. \tag{7}$$

5.1.2. Effective Stress: Basal Water Pressure

Computation of effective stress from total stresses requires estimating pore water pressure in the bed, which will depend on the water pressure in channels that bound undulations and the flux of meltwater along and through the till bed toward channels. Water production at the bed or from slightly higher in basal ice is the source of this water discharge, assuming that water from the glacier surface, as noted, tends to feed channels directly and maintain them. If the water pressures in bounding channels are treated as prescribed boundary conditions, then steady water pressure in interfluve areas can be readily calculated (Figure 4). This steady water pressure is, of course, an idealization; water pressure will change in channels due to changing surface water input to them from moulins, although such pressure variations will be diffusively buffered in till pore water between channels.

To determine the water pressure, consider the same bed undulation as before in the x direction, with the origin at the base of a trough (Figure 4a). Both the basal melt rate (per unit length), $\dot{m}$, which generates water, and the till thickness, h_t, which transmits water, vary spatially, determining the form of the equation for steady flow:

$$\frac{K}{\rho_w g h_t(x)} \frac{d}{dx}\left(h_t(x) \frac{dP}{dx} \right) = -\dot{m}(x), \tag{8}$$

where $P(x)$ is the water pressure, ρ_w is the water density, and K is the depth-averaged hydraulic conductivity from the glacier sole to the base of the till, presumed to rest on bedrock of much lower conductivity so that it can be viewed as an impermeable boundary. This is a reasonable idealization at Múlajökull where basal tills consist dominantly of sand (McCracken et al., 2016) and so have a relatively high hydraulic conductivity (~10^{-6} m s^{-1}). The intimate contact between ice and the bed expected during slow, quiescent flow

(Figure 3a) inhibits preferred flow paths at the bed surface (e.g., Creyts & Schoof, 2009). Water pressures in channels at $x = 0$ and $x = \lambda$ are as follows:

$$P(0) = P_0 \tag{9a}$$

$$P(\lambda) = P_\lambda \tag{9b}$$

where P_0 and P_λ are prescribed (Figure 4a) so that the hydraulic grade line (e.g., Hooke, 2005) parallels the slope of the glacier surface. Integrating each side of equation (8) twice across the interval $(0, x)$ yields

$$P(x) = -\frac{\rho_w g}{K}\int_0^x\left(\frac{1}{h_t(x)}\int_0^x \dot{m}(x)h_t(x)\mathrm{d}x\right)\mathrm{d}x + \frac{h_t \mathrm{d}P}{\mathrm{d}x}|_{x=0}\int_0^x \frac{1}{h_t(x)}\mathrm{d}x + P_0, \tag{10}$$

but with the value of $\frac{h_t \mathrm{d}P}{\mathrm{d}x}|_{x=0}$ unknown. Solving for it by using equation (9b) to set P_λ equal to right-hand side of equation (10) with $x = \lambda$ and then substituting the result into equation (10) yield the water pressure:

$$P(x) = P_0 - \frac{\rho_w g}{K}\int_0^x F\,\mathrm{d}x + \left(\frac{P_\lambda - P_0 + \frac{\rho_w g}{K}\int_0^\lambda\left[\frac{1}{h_t(x)}\int_0^\lambda \dot{m}(x)h_t(x)\,\mathrm{d}x\right]\mathrm{d}x}{\int_0^\lambda \frac{1}{h_t(x)}\mathrm{d}x}\right)\int_0^x \frac{1}{h_t(x)}\mathrm{d}x, \tag{11}$$

with

$$F = \frac{1}{h_t(x)}\int_0^x \dot{m}(x)h_t(x)\,\mathrm{d}x. \tag{12}$$

The till thickness $h_t(x)$ is the mean till thickness, h, added to the variation due to the height of undulations (equation (1)):

$$h_t(x) = h - a\cos\left(\frac{2\pi x}{\lambda}\right) \tag{13}$$

(Figure 4a). Equations (8), (9a), (9b), (10), (11), (12), and (13) are also applicable to undulations along profiles perpendicular to flow (Figure 4b), although in that case, $P_0 = P_\lambda$.

Integrating equation (12) to obtain $P(x)$ from equation (11) requires knowing the rate of basal water production by melting, $\dot{m}(x)$. As ice deforms over bed undulations during sliding, it dissipates a heat flux per unit area, q_s. We assume that this heat dissipation is uniform along undulations, although this idealization is strictly correct only for linearly viscous ice (Kamb, 1970). Geothermal heat also melts ice. Hooke and Medford (2013) recently emphasized how lateral variations in geothermal heat flux associated with bed topography might help promote local freezing at the bed and associated drumlin growth. Although Múlajökull is a fully temperate glacier, herein we consider whether such heat-flux variability could affect the basal distribution of melting sufficiently to alter effective stress patterns. Thus, assuming that all heat melts ice either at the ice sole or in the basal ice layer, the melt rate is

$$\dot{m}(x) = \frac{1}{\rho L}(q_s + q_G + \Delta q_G(x)), \tag{14}$$

where L is the latent heat of ice, q_G is the mean geothermal heat flux per unit area (~0.15 W m^{-2}; Hjartarson, 2015), and $\Delta q_G(x)$ is a heat flux deviator that reflects how the geothermal heat flux varies with position on the bed. The heat flux from sliding, q_s, is the product of the basal velocity, u, and shear stress, τ. Lliboutry (1979, equation (85)) showed that the distribution of normal stress on undulations indicated by equations (2) and (3) yields

$$\tau = \left(\frac{e}{2}\right)^{(n-1)/n}\left(\frac{u\pi}{A\lambda}\right)^{1/n}\left(\frac{2\pi a}{\lambda}\right)^{(n+1)/n}. \tag{15}$$

Thus,

$$q_s = \left(\frac{e}{2}\right)^{(n-1)/n}\left(\frac{\pi}{A\lambda}\right)^{1/n}\left(\frac{2\pi u a}{\lambda}\right)^{(n+1)/n}. \tag{16}$$

The spatial variation in geothermal heat flux reflects the variation in ice normal stress on the bed, which causes the pressure-melting temperature of the ice to vary along the surfaces of undulations (e.g., areas under higher pressure are colder and hence receive higher heat fluxes). As shown in Appendix A, the deviation from the mean geothermal heat flux is approximated by

$$\Delta q_G(x) = K_t C\left[\rho g(H_0\phi_c + a)\frac{2\pi}{\lambda}\cos\left(\frac{2\pi x}{\lambda}\right) + A' u^{1/n}\frac{2\pi}{\lambda}\sin\left(\frac{2\pi x}{\lambda}\right)\right], \tag{17}$$

where C is the depression of the melting point of ice with pressure and K_t is the thermal conductivity of the till bed. Equations (14) and (17) neglect the effects of, respectively, heat dissipation and advection in water flowing toward channels. Equations (13), (14), (16), and (17) allow the numerical integration of equations (11) and (12) to obtain $P(x)$, which when subtracted from the total normal stress (equation (6)) yields the distribution of effective stress in an along-flow profile:

$$N(x) = \sigma_t(x) - P(x). \tag{18}$$

For transverse profiles (Figure 4b), with ice flow directed parallel to the crests of undulations, $N(y)$ is computed in the same way, except that the total normal stress, $\sigma_t(y)$, is given by equation (7) and thus neglects normal stresses that depend on sliding, and $P(y)$ is computed without consideration of the effect of sliding on the deviation from the mean geothermal heat flux (the term in equation (17) that contains u is neglected). Importantly, the heat dissipated by sliding ice is retained in equation (14), despite undulations with their crests oriented parallel to flow, to better approximate conditions along a transverse profile through the crest of an actual three-dimensional undulation.

5.1.3. Till Entrainment in Temperate Ice

Rempel (2008) showed that even under modest effective normal stress on subglacial till, ice will infiltrate it, so that a transitional zone that contains a mixture of ice, water, and sediment particles should commonly characterize the base of the glacier. If pores between till grains are sufficiently large and ice is in intimate contact with the till surface such that no intervening layer of through-flowing water exists, this "frozen fringe" develops because intermolecular forces within it are necessary to support the overburden pressure of the ice in excess of the till pore water pressure (Figure 3a). This fringe with entrained sediment particles will develop even beneath a temperate glacier that is melting at its base. The thickness of the fringe depends on the relationship between its temperature and the extent to which the pores of the till are filled with ice, which depends on the pore geometry. Although this relationship is known empirically for some soils, no such data are available for tills.

Rempel (2008), however, provided simple approximations for bounding values of the steady thickness of the fringe, h_f, under a steady effective normal stress, when the temperature–ice saturation relationship is poorly known. If the temperature gradient across the frozen fringe, G_f, is simplified as uniform, then

$$\frac{N - p_f}{(1 - n_t)(\rho_r - \rho_w)g - G_f\rho L/T_m} \le h_f \le \frac{N - p_f}{(1 - n_t)[(\rho_r - \rho_w)g - G_f\rho L/T_m]}, \tag{19}$$

where n_t is the till porosity, ρ_r is the rock particle density, T_m is the bulk melting temperature of ice at atmospheric pressure, and p_f is a threshold pressure that causes a temperature depression sufficient to allow freezing in the pore spaces. This pressure depends inversely on pore size; for silty, sandy tills with little clay, such as those at Múlajökull, it is modest with $p_f = O(10^4)$ Pa (Rempel, 2008). $G_f = q/K_f$, where q and K_f are, respectively, the heat flux through the fringe and its bulk thermal conductivity. The left-hand and right-hand sides of equation (19) correspond to the end-member cases in which ice saturation of the pores is zero and 100%, respectively. The two terms in the denominators are vertical pressure gradients required for static stress equilibrium in the frozen fringe: the left-hand term is caused by the buoyant weight of the rock particles in the water film that surrounds it, and the right-hand term reflects the hydraulic gradient that drives interfacial water to where ice is coldest and water films are thinnest. This latter effect, called the thermodynamic buoyancy (Rempel et al., 2001), depends on the extent of pore saturation by ice. These forces operate over the thickness of the fringe, so that thicker fringes are necessary to support larger effective stresses.

Rempel (2008) advocated use of the lower bound of equation (19) in estimating h_f because even when ice resides between soil particles, interfacial water tends to occupy much of the pore space. Use of this lower bound also, however, requires evaluating how it would be affected by basal melting, which is assumed to

be zero in the derivation of equation (19). Considering basal melting results in a third term in the denominator of the lower bound that depends the basal melt rate but that is orders of magnitude smaller than the other two terms (Appendix B). Results of Rempel's less idealized calculations of h_f, which include temperature-dependent ice saturation and a nonuniform temperature gradient across the fringe, are, likewise, insensitive to the value of the basal melt rate. Thus, a good approximation is to use the lower bound of h_f to estimate the steady fringe thickness, with no additional term dependent on the rate of basal melting.

Unfortunately, the lower bound of equation (19) alone is inadequate because the full steady-state thickness of the fringe is not likely achieved during the typical duration of a surge cycle's quiescent phase at Múlajökull (of order 10 years). Rempel (2008) calculated time-dependent changes in fringe thickness in response to abrupt increases in effective normal stress and found that the time required for these changes increased with the magnitude of the stress increase and can be of order 100 years. To avoid discretizing the frozen fringe to numerically compute its transient thickness (Rempel, 2008), we adopt a cruder but simpler alternative that uses the lower bound of equation (19) to estimate the transient thickness, h_{ft}, of the fringe at the end of a quiescent phase:

$$h_{ft} = c_t \frac{N - p_f}{(1 - n_t)(\rho_r - \rho_w)g - G_f \rho L / T_m}, \tag{20}$$

where c_t is a constant between 0 and 1 that depends on the magnitude of the average, post-surge, effective stress increase and on the duration of the quiescent phase. The value of c_t can be roughly estimated from the results of Rempel (2008) or estimated more precisely by repeating his calculations for pertinent parameter values. Thus, at the end of a quiescent period, thicknesses of till equal to h_{ft} and dependent on spatial variations in effective normal stress are entrained in ice and eroded from the bed surface.

5.2. Surging

Surging is expected to be accompanied by development of an inefficient, distributed drainage system at the bed, an associated reduction in effective normal stress on the bed, and pervasive shearing of the till substrate. Slip resistance at the bed, therefore, transitions from form drag during quiescent flow, associated with slip over a rigid bed, to a shear stress, τ_s, during surging limited by the Coulomb strength of the shearing substrate:

$$\tau_s = N_s \tan \phi_u, \tag{21}$$

where N_s is the effective normal stress during surging and ϕ_u is the ultimate friction angle of till sheared sufficiently to have attained a steady porosity. Cohesion is excluded because it is likely zero in highly strained sediments lacking clay (Mitchell, 1993). In reality, N_s may vary across undulations, for example, as a result of form drag that may persist even in the presence of bed deformation. Overpressuring and underpressuring on undulations will be significantly reduced, however, relative to the rigid bed case, owing to frictional resistance at the bed that helps balance the basal drag. Moreover, there is not an obvious rationale for predicting spatial variations in basal water pressure during a surge that would be necessary to compute spatial variations in N_s. Thus, as a null hypothesis, N_s is considered to be uniform during surging.

Through-flowing water across a large fraction of the bed surface during surging and low effective stress relative to quiescence likely shut off the Rempel (2008) till entrainment mechanism. The frictional heat flux caused by deformation of the bed is $q_d = u_s \tau_s$, where τ_s is provided by equation (21) and u_s is the slip velocity associated with surging. Together with the geothermal heat flux, this heat causes vigorous melting of the glacier base and release of debris that deposits from the frozen fringe a layer of till on the bed (Figure 3b). Also, the volumetric flux per unit width of till that moved in the deforming bed, Q_D (including porosity), may change downglacier causing erosion or deposition. Over a surge duration, t_s, a till layer of thickness, D, is deposited:

$$D = \frac{t_s n_t}{\rho L I_f^2} (u_s N_s \tan \phi_u + q_G) - t_s \frac{dQ_D}{dx}, \tag{22}$$

where I_f is the volume fraction of ice in the frozen fringe (for larger values of I_f, more heat is required to melt a given thickness of debris-bearing ice per unit time from the glacier sole and less debris is accreted on the bed for a given thickness melted). Equation (22) resembles the Exner equation (e.g., Paola & Voller, 2005). Spatial variations in geothermal heat flux, like those considered during quiescent flow (equation (17)) are neglected

Table 1
Parameter Values

Parameter	Symbol	Value
Flow law coefficient	A	2.4×10^{-24} Pa^{-3} s^{-1}
Ice melting point depression due to pressure	C	7.42×10^{-8} K Pa^{-1}
Coefficient for transient frozen fringe	c_t	0.2
Mean ice thickness	H_0	200 m
Ice volume fraction of frozen fringe	I_f	0.65
Till hydraulic conductivity	K	10^{-6} m s^{-1}
Frozen fringe thermal conductivity	K_f	2 W m^{-1} K^{-1}
Till thermal conductivity	K_t	2 W m^{-1} K^{-1}
Till permeability	k	2×10^{-13} m^2
Crevasse scaling parameter	k_c	4
Latent heat of ice	L	3.34×10^5 J kg^{-1}
Flow law exponent	n	3
Till porosity	n_t	0.30
Threshold pressure for regelation infiltration	p_f	10,000 Pa
Geothermal heat flux	q_G	0.15 W m^{-2}
Channel pressure head to ice thickness ratio (quiescence)	R_P	0.65
Basal water pressure head to ice thickness ratio (surging)	R_N	0.80
Bulk melting temperature of ice at atmospheric pressure	T_m	273 K
Surge duration	t_s	1.0 a
Quiescent slip velocity	u	12 m a^{-1}
Surge slip velocity	u_s	400 m a^{-1}
Glacier slope	α	0.03
Channel spacing	λ	300 m
Till peak friction angle	ϕ_p	35°
Till ultimate friction angle	ϕ_u	34°
Water viscosity	η	0.0018 Pa s
Ice density	ρ	920 kg m^{-3}
Rock particle density	ρ_r	2,700 kg m^{-3}
Water density	ρ_w	1,000 kg m^{-3}
Flux divergence in deforming bed during surging	dQ_D/dx	0 m a^{-1}

in equation (22) because they are negligibly small during surges. During surges, with increases in basal slip velocity of one to two orders of magnitude, the frictional heat flux greatly exceeds the geothermal flux and especially its spatial variation.

5.3. Model Limits on Drumlin Height

If drumlins grow too high at a prescribed sliding speed, some of the model assumptions break down. During quiescent flow, both the shear stress on drumlins and heat flux associated with sliding increase with $a^{(n+1)/n}$ (equations (15) and (16)), remembering that during quiescence the bed is rigid. Increased heat flux increases meltwater generation, causing basal water pressures to increase and reducing the effective normal stress on the bed. Thus, growth of drumlins both decreases the strength of till within them and increases the drag that sliding ice exerts on them. If $\overline{N}$ is the average effective normal stress on the bed along a drumlin, ϕ_p is the peak friction angle of the till, and c is its cohesion, then the assumption that drumlins are rigid requires that

$$\tau < \overline{N} \tan \phi_p + c, \tag{23}$$

where τ is shear stress on a drumlin given by equation (15) and the right-hand side is the Coulomb strength of the till. At a given slip velocity, this criterion is violated once drumlins exceed a particular amplitude.

Similarly, as drumlins increase their amplitude, the assumption that ice everywhere maintains contact with the bed breaks down. If locally $\sigma_t \geq P$, ice will remain in contact with the bed (see also Schoof, 2007). However, as amplitude increases, underpressuring associated primarily with sliding but also with crevasse formation at the glacier surface will cause this condition to be violated in the lees of undulations, implying that cavities should form there.

The extent to which either of these criteria may help limit the heights of actual drumlins is unclear. Nevertheless, because either deformation of undulations or ice-bed separation during quiescence make some of the model's relationships unjustifiable, calculations of drumlin evolution are stopped once drumlins reach an amplitude at which either criterion is violated.

6. Parameter Choices and Results

During a succession of surge cycles, each quiescent phase causes a distribution of erosion set by the effective stress (equation (20)), and each surge causes deposition (equation (22)). Parameter values are listed in Table 1. Particularly, important prescribed parameters are the channel spacing, which sets the lengths and widths of incipient drumlins, and the water pressure in channels, which sets the upper limit on effective stress during quiescent flow. The channel spacing is chosen to crudely reflect the spacing of drumlins in the forefield, which in turn reflects the spacing of channel portals at the glacier margin. Water pressure in channels is specified using the ratio of pressure head to ice thickness, $R_P = P_0/\rho_w gH$. Similarly, effective normal stress during surging is specified through the ratio of basal water pressure head to ice thickness: $R_N = (\rho/\rho_w) - (N_s/\rho_w gH)$. A large till hydraulic conductivity is considered, consistent with the coarse texture of the Múlajökull till (McCracken et al., 2016). Slip velocities during quiescence and surges are prescribed. No attempt is made to couple drumlin height to slip velocity, given that near the margin slip velocity is likely sensitive to upstream ice dynamics. Surge velocities have not been measured at Múlajökull, so values are used that fall within ranges measured for some other Icelandic glaciers (Björnsson et al., 2003). The value of c_t (equation (19)) is estimated roughly based on Rempel's (2008) calculations of transient frozen-fringe thickness and average periods between surges at Múlajökull. A value of the scaling factor, k_c (equation (5)), is specified to result in peak depth-averaged ice porosities from crevasses of 0.005–0.08, across the full range of drumlin amplitudes considered. During surges when the bed shears, zero downglacier flux divergence due to bed

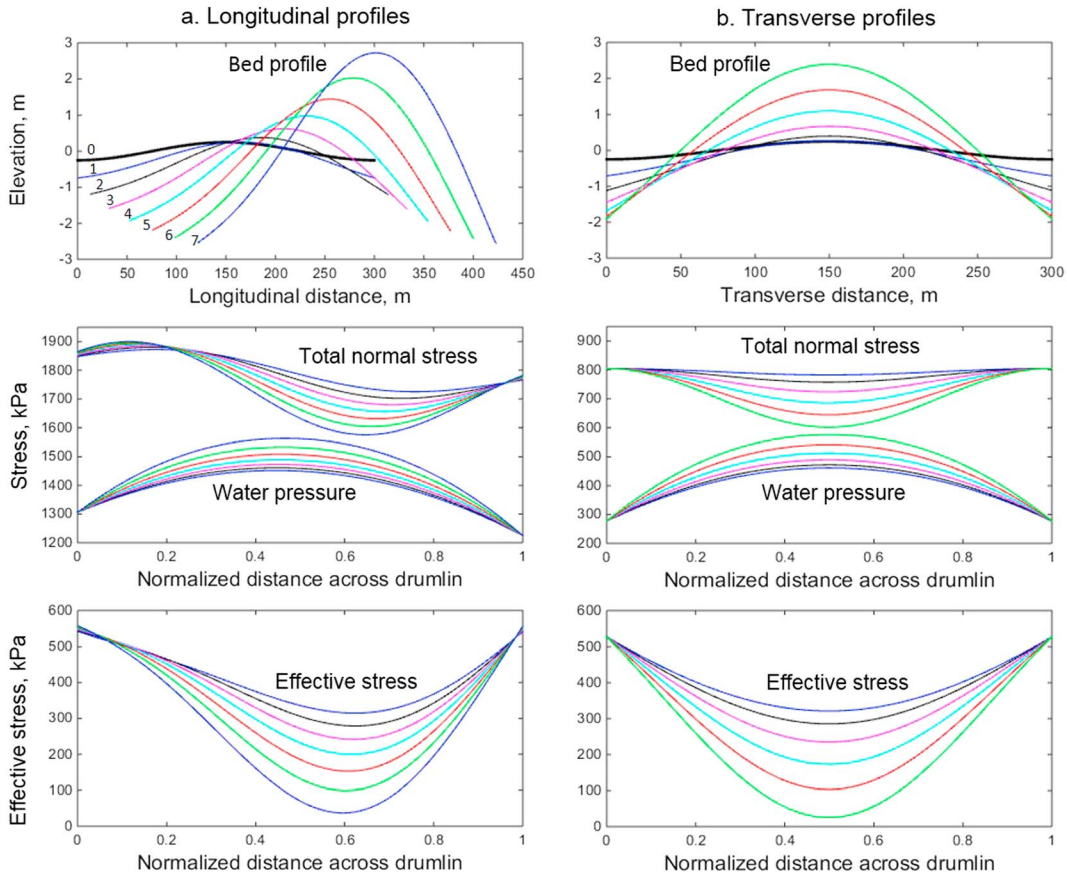

Figure 5. Model bed profiles and stresses as a function of distance in (a) longitudinal and (b) transverse sections, with each colored line representing conditions after a successive surge. Parameter values for calculations are listed in Table 1. Heavy black lines show the initial bed undulation (a = 0.25 m), which is superimposed on a layer of till of initial mean thickness, h = 24 m. Numbers in the top panel of Figure 5a indicate profiles after successive surge cycles, with the color coding the same in the other plots of the figure. Different numbers of surge cycles are required to reach the limiting drumlin height in the longitudinal and transverse cases because calculations in the two directions are not coupled.

deformation (dQ_D/dx) is prescribed in equation (22), as a null condition and consistent with AMS fabrics at Múlajökull that do not indicate compressional or extensional strains (McCracken et al., 2016).

Results illustrate how and why gentle bed undulations (a = 0.25 m, λ = 300 m) grow in the model (Figure 5). Erosion during quiescent flow is greatest near channels, where effective stress is highest. In the along-flow direction, erosion rates are smallest downglacier from crests of undulations. There, the effects of low ice pressure due to sliding and to a lesser extent crevasse formation combine with high water pressure to cause a minimum in effective stress (Figure 5). When combined with uniform deposition during surges, this effective stress distribution during quiescent flow causes drumlins to accrete on their lee sides while their stoss sides are eroded, resulting in bedform growth and downstream migration (Figure 5a).

Rates of growth of drumlins increase as their amplitude increases (Figure 5). Sliding and crevasse formation cause ice pressure gradients that increase with drumlin amplitude. Also, taller drumlins generate more frictional meltwater that must be conveyed to channels, resulting in larger differences in pore water pressure from the centers of drumlins to their edges. These feedbacks combine to make effective-stress gradients across drumlins during quiescence increase with drumlin amplitude. Resultant erosion causes topographic perturbations to grow unstably. The effect of gradients in basal ice temperature, which increasingly deflect flow of geothermal heat and focus basal melting as drumlins grow, is minor; resultant spatial variations in geothermal heat flux are less than 1% of the mean value. Eliminating this effect in the calculation for the reference case of Figure 5 changes effective stresses by less than 2%. Unstable growth in the reference

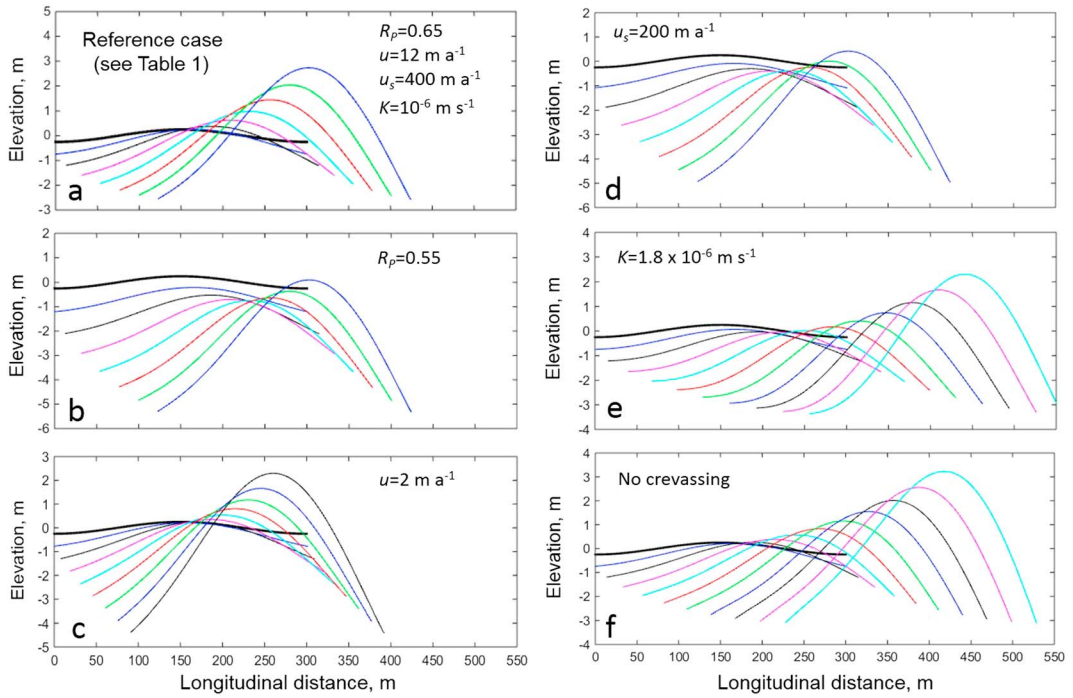

Figure 6. Longitudinal profiles along model drumlins for the (a) reference set of parameters (Table 1); for a (b) channel pressure head to ice thickness ratio, $R_P = P_0/\rho_w gH$, reduced to 0.55; (c) slip velocity during quiescent flow, u, reduced to 2 m a^{-1}; (d) slip velocity during surges, u_s, reduced to 200 m a^{-1}; (e) till hydraulic conductivity, K, increased to 1.8×10^{-6} m a^{-1}, and (f) for the case of no crevasses on the glacier surface above drumlins. Colored lines indicate profiles after successive surges, and heavy black lines show the initial bed undulation (a = 0.25 m; h = 24 m).

case of Figure 5a is stopped after seven surge cycles when equation (23) is no longer satisfied, and the bed is no longer rigid.

Regardless of how parameters are varied in the model, initially gentle perturbations grow unstably, but how drumlins evolve can vary widely (Figure 6). Decreasing water pressure in channels by only 15% (R_P = 0.65 to R_P = 0.55) during quiescent flow, relative to the reference case of Figure 5, creates drumlins in a regime of net erosion (Figure 6b), owing to higher effective stress that accelerates debris entrainment. A more erosional drumlin-forming environment is also caused by a decrease in quiescent slip velocity (Figure 6c), which results in less frictional meltwater being conveyed to channels, lower pore water pressures, and higher effective stresses. Similarly, a 50% reduction in slip velocity during surging causes drumlin formation to be accompanied by severe erosion over multiple surge cycles (Figure 6d), owing to lower rates of frictional heat dissipation, lower rates of basal melting, and less resultant deposition on the bed during surges. Erosion can also be more prevalent if hydraulic conductivity of the bed is higher (Figure 6e), reducing hydraulic gradients toward channels and pore water pressures. Undulations still grow in the absence of the crevassing feedback, but growth is slowed (Figure 6f).

Drumlin development accompanied by major aggradation can result if the debris flux from bed deformation during surges—assumed in the reference case (Figure 5) to be spatially uniform—decreases downglacier. For example, considering $dQ_D/dx = -0.3$ m a^{-1} (equation (22)) causes aggradation with only minor erosion of the initial undulating, predrumlinized surface (Figure 7a). Considering a still larger value, $dQ_D/dx = -1.0$ m a^{-1}, results in no net erosion of that surface during drumlin development. Even stoss surfaces aggrade in that case because the rate of aggradation exceeds the rate of bedform migration (Figure 7b).

The model predicts a characteristic stratigraphy. In longitudinal sections, modeled layers dip gently downglacier and parallel with the lee surfaces of drumlins (Figure 8a). On the upstream sides of drumlins, layers either can be unconformable with a surface layer of till, if the last event to affect the stratigraphy was a surge, or can simply intersect the drumlin surface at an angle, if sustained quiescent flow was the last event to affect the stratigraphy. The former situation is depicted in Figure 8 because the last surge at Múlajökull in 2008 left a till

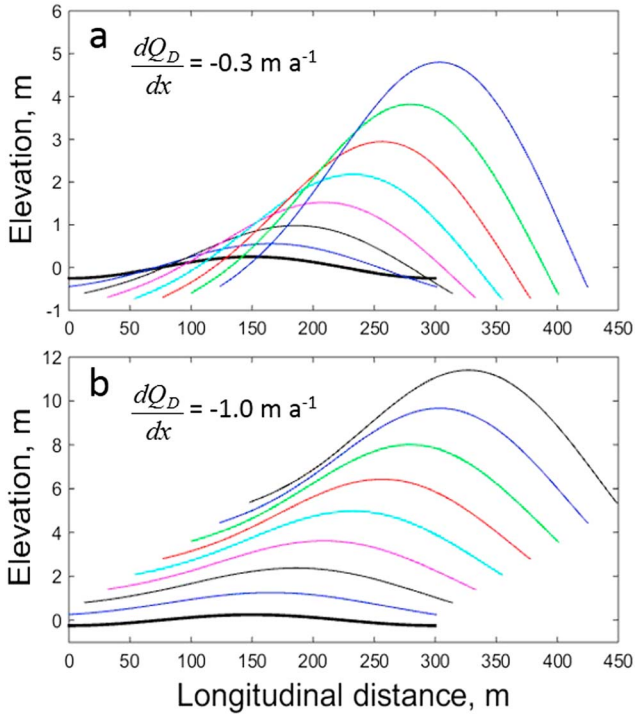

Figure 7. Drumlin profile development if till flux in a deforming bed during surges decreases downglacier (negative flux divergence, dQ_D/dx): (a) $dQ_D/dx = -0.3$ m a^{-1} and (b) $dQ_D/dx = -1.0$ m a^{-1}. Colored lines indicate profiles after successive surges, and heavy black lines show the initial bed undulation (a = 0.25 m; h = 24 m).

of roughly uniform thickness draped over the part of the forefield overridden by the surge. In transverse sections, angular unconformities are expected on parts of drumlin flanks (Figure 8b), with unconformities increasingly prominent in drumlins that form under more erosional regimes. Unconformities at drumlin heads and flanks are not always predicted by the model: if rates of till deposition by bed deformation during surges are sufficiently large, erosion on the stoss sides and flanks of drumlins will not accompany drumlin growth and migration (Figure 7b). Unconformities may also occur at depth where drumlin tills accumulate on the eroded parts of predrumlin topography (e.g., Figure 8a).

7. Discussion

7.1. Model Strengths

The primary strength of this model is that it stems from a large, specific set of observations from an active drumlin field (Benediktsson et al., 2016; Johnson et al., 2010; McCracken et al., 2016). The model formulation reflects the following conclusions from observations at Múlajökull:

1. Drumlins develop progressively over multiple surge cycles.
2. Surges deposit individual basal till units, so the bed aggrades during surges.
3. Till layers are deposited on drumlin topography, so deposition occurs during rather than before drumlinization.
4. Till layers are deposited in shear, and shear azimuths and planes mimic the drumlin topography, also indicating that deposition occurs during rather than before drumlinization.
5. Erosion occurs at the heads and flanks of drumlins, increasing their relief.
6. The last surge deposited a till that drapes both drumlins and intervening areas, suggesting that erosion occurs during quiescent flow.
7. Subglacial channels during quiescent periods tend to occupy low areas between drumlins.
8. Basal effective stress during quiescent periods is sufficiently higher between drumlins than within them to indicate that subglacial water moves toward low areas between drumlins.
9. Crevasses near the terminus during quiescence are coincident with underlying drumlins.

A model of drumlin formation anchored to such observations has better potential to approximate reality than one that lacks such guidance. On the other hand, the extent to which such a model can be applied to drumlins elsewhere is an open question and one that will be difficult to address without comparable data from other drumlin fields.

Another strength of the model, also aimed at optimizing its physical relevance, is that only parameters that can be either independently measured or estimated are used in it. For example, the model does not include till viscosity as a parameter because under steady conditions the shear stress that till supports is highly insensitive to its strain rate (e.g., Kamb, 1991; Iverson et al., 1998; Tulaczyk et al., 2000), such that if a power law rheology is fit to data, stress exponents are either greater than 60 or negative (e.g., Iverson, 2010). Thus, tills are best idealized as plastic materials (e.g., Cuffey & Paterson, 2010), and although the meaning of viscosity in other contexts is, of course, unambiguous, its use to describe till deformation is problematic (Iverson, 2003).

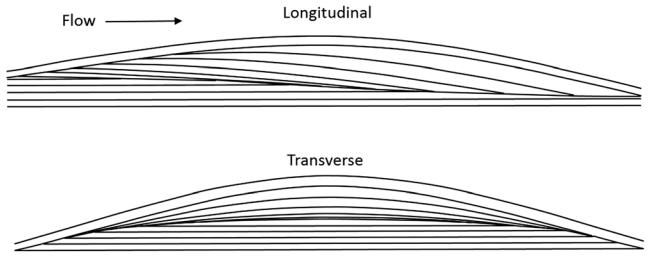

Figure 8. Model drumlin stratigraphy in longitudinal and transverse sections for the reference set of parameters (Table 1, see also profiles of Figure 5). Flat-lying layers are predrumlin sediments.

The model, for the ranges of parameters considered, produces final drumlin amplitudes (Figures 5 and 6) in the middle of the range observed at Múlajökull (Benediktsson et al., 2016) and over a number of surge cycles that roughly agree with the post-Little Ice Age surge

history of Múlajökull. These amplitudes reflect the criterion that drumlin growth stops if shear stresses during basal slip equal the average shear strength of the drumlin till. Preferential shear deformation of drumlins when they reach a certain height might indeed, through redistribution of sediment toward low areas between drumlins, offset the differential erosion during quiescent flow that causes drumlin relief to increase in the model. A process like this is seemingly necessary to counteract the instability that causes drumlins to grow at an increasing rate. Crevasse swarms above drumlins, which become increasingly extensive as drumlins grow, speed drumlin growth but are not essential for it.

More definitive than final drumlin amplitudes are the characteristic unconformities on the heads and flanks of drumlins and the low downglacier dips of till layers, all of which have been observed both directly in exposures (Benediktsson et al., 2016; Johnson et al., 2010) and with ground-penetrating radar at Múlajökull (Figure 2; Woodard, 2017). These uncomformities are usually indicated by the model, unless bed aggradation caused by negative till flux divergence in a deforming bed during surges is set sufficiently high. Unconformities at drumlin heads and conformable till layers on lee sides of drumlins reflect the erosion and deposition that causes downstream drumlin migration—a process suggested by many others (e.g., Boulton, 1987; Menzies, 1986; Piotrowski, 1989). Downstream migration of drumlins was produced in the reduced complexity model of Barchyn et al. (2016) by optimizing the adjustment of parameters, although the model does not include appropriate processes involving water and sediment transport (Fannon et al., 2017). Other aspects of the model stratigraphy have not been observed, such as till layers that thin systematically toward drumlin flanks (Figure 8b).

The model permits the net aggradation (Figure 5) that has accompanied drumlin formation at Múlajökull (McCracken et al., 2016). However, drumlins can form in the model either in aggradational or erosional regimes (Figures 6 and 7), depending upon relative rates of erosion during quiescent flow and rates of deposition during surges. A notable difference between this model and the conceptual model from the first study of the Múlajökull drumlin field (Johnson et al., 2010) is that both erosion and deposition in that model were attributed to the surge phase, without production of drumlin relief during quiescent flow.

If applied to nonsurge-type glaciers, the model, at face value, would predict that drumlins should form in erosional regimes. A comprehensive review of drumlin properties by Eyles et al. (2016) led them to conclude that most drumlins indeed form in erosional regimes, although the process invoked in their analogy-based, conceptual model—abrasion at the base of a deforming layer—differs from the processes proposed here. As noted by many others (e.g., Gravenor, 1953; Menzies, 1979; Stokes et al., 2011; Vreeland et al., 2015), the diverse internal compositions of drumlins are generally more consistent with relief caused by erosion rather than by deposition. Erosional hypotheses, however, need to account for large volumes of sediment evacuated from the bed. In addition, some observations from Pleistocene drumlin fields where evidence for surging is lacking indicate that drumlin relief partly reflects depositional processes (e.g., Ellwanger, 1992; Goldstein, 1994; Stea & Brown, 1989; Whittecar & Mickelson, 1977). These field observations highlight that confining sediment transport processes during quiescent flow to only the Rempel (2008) entrainment mechanism, as does our model, is an idealization that, although convenient, excludes other mechanisms of sediment transport that likely operate during normal glacier flow.

7.2. Model Weaknesses

A weakness of the model shared by most other quantitative drumlin models (e.g., Fowler, 2010; Hindmarsh, 1998; Hooke & Medford, 2013) is that it does not consider processes in three dimensions. Drumlin development is considered in longitudinal and transverse planes (Figure 5) with depth averaging, but processes in these planes are not coupled. Solving, for example, a generalized version of equation (8) along both x and y to determine the distribution of basal water pressure is readily done with a finite-difference scheme; this reduces pore water pressures in the bed under otherwise identical conditions (Iverson et al., 2016) but does not inhibit the drumlin-forming instability. More difficult, however, would be computing the ice pressure field on a three-dimensional undulation resulting from basal slip. Reluctance to bring a full-Stokes, finite-element code to bear on this problem—and so mount a rocket engine on the bicycle that is our simple model—led us to not yet try to address the three-dimensional problem.

A liability of not considering three-dimensional undulations is that supply-limited deposition from ice during surging cannot be meaningfully included in the model. Debris supply in the ice during a surge, at a given

position and time along an undulation, will depend on the thickness distribution of debris entrained in the frozen fringe along a flow line upstream. Thus, debris supply will depend on how undulations are located relative to each other on the bed surface.

Unlike bed-shear instability models, this model does not begin with a featureless bed or focus on development of preferred length scales due to instability. Rather, the specified spacing of subglacial channels sets the length scales of drumlins. Our model is, in this way, analogous to models of erosional glacial landscape evolution (e.g., Pedersen & Egholm, 2013) where preexisting river patterns set the length scales for valley spacing, and the focus is on processes that amplify relief.

Additional complexity could be added to this model by combining it with a hydrological model to allow the channel spacing and water pressure to evolve to steady values as free parameters (e.g., Werder et al., 2013), rather than being prescribed. Such a model would need to include unknown water discharges from upstream on the bed and from moulins near the glacier margin. Thus, although this approach would avoid prescribing channel spacing, it would carry with it the liability of prescribing parameters that are equally or more poorly known. Our observations, on the other hand, include evidence for channel locations. The scope of the model, therefore, fits the scope of our observations.

A fundamental limitation of this model and other drumlin models is that the relative roles of possible sediment transport mechanisms are assumed, rather than inferred definitively from observations. Till deformation that occurs near the bed surface during lodgment of debris (Boulton et al., 1974; Larsen et al., 2004; Piotrowski et al., 2004; Tulaczyk, 1999) makes distinguishing debris transported primarily in ice difficult or impossible to distinguish from debris transported in a shearing bed (e.g., Evans & Hiemstra, 2005). To evaluate debris entrainment in ice, we have used the regelation infiltration model of Rempel (2008) as a physically complete description of how temperate ice entrains debris from a soft bed. However, as noted, other processes can, of course, cause erosion or aggradation (e.g., Alley et al., 1997). Potential erosion by water in subglacial channels is neglected and could be substantial; observations at Múlajökull rule out fluvial erosion only on the grand scale envisioned by Shaw (2002; Johnson et al., 2010).

7.3. Comparison With Other Quantitative Models

In other quantitative models aimed at describing drumlin formation beneath warm-based glaciers, local till flux divergence causes relief. This includes the reduced complexity model of Barchyn et al. (2016); however, owing to the high degree of parameterization of sediment transport and hydrological processes in that model, we do not consider it further here. In the model of Boulton (1987), effective stress on till and its associated shearing resistance are highest within drumlins, providing patches of less deformable till for nucleating drumlin growth. Similarly, in the bed-shear instability model of Fowler and Chapwanya (2014), pooling of water between drumlins in zones of zero effective stress provides the transverse component of drumlin relief (Fowler & Chapwanya, 2014). Till squeezes in a deforming bed away from higher effective stresses at drumlin long axes and toward the pooling water, which transports the debris downglacier.

Till density and preconsolidation data indicate that these hypotheses can be rejected at Múlajökull (McCracken et al., 2016). Maximum effective stresses were higher between drumlins than within them, the opposite of that assumed in these models. Whether the measured effective stress distribution is representative of other drumlin fields is unknown because field studies of drumlin materials have not focused both on relevant geotechnical properties of sediment and on both drumlin and interdrumlin areas (see, for example, the review by Stokes et al., 2011). Testing contrasting models should be a priority, so future field work would benefit from such measurements.

AMS fabrics, complemented by traditional clast fabrics, do not support the bed shear instability model of Fowler and Chapwanya (2014) at Múlajökull. These data, contrary to that model, indicate no general tendency for till shearing away from drumlin long axes toward low areas between drumlins where water layers in that model reside. Rather, fabrics indicate mildly divergent and convergent shear of till along, respectively, stoss and lee surfaces of drumlins (McCracken et al., 2016).

Both in this model and in the bed-shear instability model, small perturbations in bed topography set up feedbacks that cause perturbations to grow. Interestingly, in both models the same effect is responsible for the instability along a flow line: the gradient in total normal stress on the bed that arises from basal slip. In the

case of the new model, this effect, together with decreases in pore water pressure toward channels, causes effective stresses and erosion during quiescent flow that are minimized on lee surfaces and maximized near channels, causing undulations to both migrate downglacier and grow in amplitude as surge cycles progress. In the case of bed shear instability models, high pressure on stoss surfaces is assumed to increase the till flux there by bed shear. The higher flux can arise due to an increase in till viscosity with pressure (e.g., Schoof, 2007). If the bed is shearing, ice is coupled to the bed surface, and velocity there is uniform, the higher till viscosity on stoss surfaces causes larger shear stresses. Considering till to be a linearly or nonlinearly viscoplastic fluid, in which shear stress above a threshold value is proportional to the till flux by bed deformation, leads then to higher till fluxes into undulations than out of them, causing them to grow in amplitude (e.g., Schoof, 2007). In the most recent version of the bed shear instability model (Fannon et al., 2017), the authors attribute the same flux imbalance to a dependence of deformation depth on effective pressure. The till viscosity is taken to be a constant.

The new model, in addition to being consistent with measured effective stress gradients and till deformation kinematics, avoids assigning a viscosity or viscous properties to till. As noted, the empirical evidence for doing so is weak (Cuffey & Paterson, 2010; Iverson, 2010). More importantly, the central assumption of bed shear instability models—that the debris flux in a subglacially deforming till layer is higher where effective stresses are higher—has been only hinted at rather than demonstrated. Numerical simulations with the discrete element method, in which depths of shear deformation were larger at higher total normal stresses, support this dependence (Damsgaard et al., 2013). However, the significance of this result is uncertain because in these simulations till particles were idealized as spherical and of uniform size, pore water and its flow were neglected, and most importantly, shear zones were only one order of magnitude thicker than the grain size. On the other hand, some field observations of instrumented subglacial tills also indicate that reductions in effective stress can decrease deformation depth, at least transiently (e.g., Boulton et al., 2001; Iverson et al., 2007).

8. Conclusions

We suggest a new drumlin-forming instability. For the case considered here of a surge-type glacier, slip of ice across topographic perturbations during quiescent flow, together with flow of water toward bounding channels, causes an effective-stress distribution on the bed that erodes the flanks and heads of drumlins preferentially by regelation infiltration. Other potential mechanisms of erosion that are not included in the model, such as fluvial erosion in subglacial channels, could contribute to this effect. Surges deposit till on and between drumlins, the extent of which helps control whether drumlins form during net aggradation or erosion of the bed. Both the advective flux of till due to its shear deformation during surges and lodgment of debris on the bed during surges result in till fabrics indicative of shear. Drumlins grow increasingly rapidly and migrate downglacier over multiple surge cycles. In the absence of surging, the model describes how drumlins may form in a purely erosional regime (e.g, Eyles et al., 2016).

The model differs from other quantitative models because it is both constrained by field observations at an active drumlin field and contains only parameters that can be measured or estimated. The model can also be readily tested because it provides a quantitative prediction of drumlin stratigraphy and defines permissible distributions of effective stress and patterns of till strain, both of which can be inferred from field observations (e.g., McCracken et al., 2016).

Appendix A: Spatial Variation of Geothermal Heat Flux

The geothermal heat flux will be preferentially focused on cold parts of the bed and deflected away from warm parts. Ice is everywhere at its melting temperature, so the normal stress variation on the bed (equation (6)) controls the temperature variation. Neglecting the small variation in normal stress due to the slope of the ice surface so that only other terms in equation (6) that depend on x are considered, rearranging them, and multiplying them by the temperature depression with pressure, C, yield the temperature deviation from the mean normal stress across the longitudinal profile of an undulation:

$$\Delta T_s(x) = A_1 \cos\left(\frac{2\pi x}{\lambda}\right) + A_2 \sin\left(\frac{2\pi x}{\lambda}\right). \tag{A1}$$

The left-hand term results from spatial variations in the static weight of the ice, the right-hand term is the stress variation from sliding, and the amplitudes of the temperature variations are A_1 and A_2:

$$A_1 = -C\rho g(H_0\phi_c + a), \tag{A2a}$$

$$A_2 = -CA'u^{1/n}. \tag{A2b}$$

The governing equation is

$$\frac{\partial^2 T}{\partial x^2} + \frac{\partial^2 T}{\partial z^2} = 0, \tag{A3}$$

in which $T(x, z)$ is the temperature and z is directed downward. Owing to the low slopes of drumlins, which generally are at least an order of magnitude longer and wider than they are high, we consider a semi-infinite half space, with a planar upper boundary over which temperature varies as described by equation (A1).

Consider first only the static-weight term of equation (A1) as a boundary condition. Following Turcotte and Schubert (2014, p. 177–178) yields the following solution for $T(x, z)$:

$$T(x,z) = A_1 \cos\left(\frac{2\pi x}{\lambda}\right) e^{-2\pi z/\lambda}. \tag{A4}$$

Differentiating this equation with respect to z at $z = 0$ and multiplying by the thermal conductivity of the till, K_t, yield the geothermal heat flux deviator at the bed surface that results from the spatial variation of the static weight of the ice, $\Delta q_w(x)$:

$$\Delta q_w(x) = -K_t A_1 \frac{2\pi}{\lambda} \cos\left(\frac{2\pi x}{\lambda}\right). \tag{A5}$$

Importantly, if the heat flux deviator from sliding, $\Delta q_s(x)$, can be determined independently, it can be added to right-hand side equation (A5) to determine the total spatial variation in heat flux, provided that both relations depend linearly on temperature so that the principle of superposition applies. Considering then only the second term on the right-hand side of equation (A1) as the boundary condition at the bed surface and proceeding as before yield

$$\Delta q_s(x) = -K_t A_2 \frac{2\pi}{\lambda} \sin\left(\frac{2\pi x}{\lambda}\right). \tag{A6}$$

Substituting values of A_1 (equation (A2a)) and A_2 (equation (A2b)) into the sum of the right-hand sides of equations (A5) and (A6) provides the total deviation from the mean geothermal heat flux, $\Delta q_G(x)$ (equation (17)).

Along a transverse profile, sliding does not influence the basal ice temperature, so the total spatial variation in heat flux is given by only equation (A5).

Appendix B: Effect of Basal Melt Rate on Frozen-Fringe Thickness

Rempel (2008) derived the rate of freezing, V, at the base of the frozen fringe, with negative values corresponding to rates of melting. For the case in which the temperature gradient, G_f, across the fringe is uniform, he determined (see his equation (16)) this expression for V:

$$V = \frac{{\rho_w}^2 L G_f k}{\rho T_m \eta} \left\{ \frac{T_m - T_l + n_t \int_{T_f}^{T_l} S_i dT - \frac{T_m}{\rho L}\left[N - (1-n_t)(\rho_r - \rho_w)gh_f\right]}{\int_{T_f}^{T_l} \frac{(1-n_t S_i)^2}{k_f/k} dT} \right\}, \tag{B1}$$

where k is the permeability of the till, k_f is the permeability of the frozen fringe, η is the viscosity of water, T_l is the temperature at the top of the frozen fringe, T_f is the temperature at the deepest extent of the pore ice, and S_i is the fraction of the pore space that is ice saturated. Other variables are defined as in the text. For

the limiting case in which the average value of S_i approaches zero (see text for rationale), this equation reduces to

$$V = \frac{{\rho_w}^2 L G_f k_f}{\rho T_m \eta (T_l - T_f)} \left\{ T_m - T_l - \frac{T_m}{\rho L} [N - (1 - n_t)(\rho_r - \rho_w) g h_f] \right\}. \quad \text{(B2)}$$

The threshold ice pressure required to depress the melting temperature sufficiently to freeze ice in the pore space is $p_f = \rho L (T_m - T_f)/T_m$, and the dimensionless undercooling at the glacier base is $(T_m - T_l)/(T_m - T_f) = 1 - G_f h_f/(T_m - T_f)$ (Rempel, 2008). Combining these two equations yields

$$T_m - T_l = \frac{T_m p_f}{\rho L} - G_f h_f \text{ and} \quad \text{(B3)}$$

$$T_l - T_f = G_f h_f. \quad \text{(B4)}$$

Substituting equations (B3) and (B4) into equation (B2) and rearranging terms provide a lower bound for the fringe thickness as a function of V:

$$h_f \geq \frac{N - p_f}{(1 - n_t)(\rho_r - \rho_w) g - G_f \rho L / T_m - \rho^2 \eta V / {\rho_w}^2 k}. \quad \text{(B5)}$$

This lower bound is the same as that of equation (19), except for the additional term in the denominator that contains V. Because V is negative in the case of basal melting, the effect of melting is to reduce the fringe thickness. However, considering appropriate parameter values in the three terms of the denominator (Table 1), with $G_f = q_G/K_f$, indicates that the term containing V is more than two orders of magnitude smaller than either of the other terms. Thus, the term containing V can be neglected, as in equation (20).

Acknowledgments

The Múlajökull field project was funded by the U.S. National Science Foundation (award EAR-1225812 to N. R. Iverson and award EAR-1225986 to T. S. Hooyer), the Icelandic Research Fund (RANNÍS) (grant 110237023 to Ó. Ingólfsson), as well as by grants from the University of Iceland Research Fund, the Energy Research Fund of Landsvirkjun, Iceland, the Carlsberg Foundation, Denmark, and the Royal Physiographic Society in Lund, Sweden (to Í. Ö. Benediktsson, Ó. Ingólfsson, and A. Schomacker). We thank Andrew Fowler, Chris Stokes, and two anonymous reviewers who provided helpful and thorough reviews. N.R.I. thanks the Fulbright Foundation for enabling the sabbatical leave that allowed the development of the model. Special thanks are due to all of the participants of the 2009–2015 field campaigns at Múlajökull for great company and collaboration. Results from this work are archived at Iowa State University (https://ge-at.iastate.edu/directory/neal-iverson/).

References

Alley, R. B., Cuffey, K. M., Evenson, E. B., Strasser, J. C., Lawson, D. E., & Larson, G. J. (1997). How glaciers entrain and transport basal sediment: Physical constraints. *Quaternary Science Reviews*, *16*, 1017–1038.

Ankerstjerne, S., Iverson, N. R., & Lagroix, F. (2015). Origin of a washboard moraine of the Des Moines Lobe inferred from sediment properties. *Geomorphology*, *248*, 452–463.

Barchyn, T. E., Dowling, T. P. F., Stokes, C. R., & Hugenholtz, C. H. (2016). Subglacial bed form morphology controlled by ice speed and sediment thickness. *Geophysical Research Letters*, *43*, 7572–7580. https://doi.org/10.1002/2016GL069558

Benediktsson, Í. Ö., Jónsson, S. A., Schomacker, A., Johnson, M. D., Ingolfsson, Ó., Zoet, L. K., … Stötter, J. (2016). Progressive formation of modern drumlins at Múlajökull, Iceland: Stratigraphic and morphological evidence. *Boreas*, *45*, 567–583.

Benediktsson, Í. Ö., Schomacker, A., Johnson, M. D., Ingólfsson, Ó., Geiger, A. J., & Guðmundsdótti, E. R. (2015). Architecture and structural evolution of an early Little Ice Age terminal moraine at Múlajökull, surge-type glacier, Iceland. *Journal of Geophysical Research: Earth Surface*, *120*, 1895–1910. https://doi.org/10.1002/2015JF003514

Björnsson, H., Pálsson, F., Sigurðsson, O., & Flowers, G. (2003). Surges of glaciers in Iceland. *Annals of Glaciology*, *36*, 82–90.

Boulton, G. S. (1987). A theory of drumlin formation by subglacial sediment deformation. In J. Menzies & J. J. Rose (Eds.), *Drumlin Symposium* (pp. 25–80). Rotterdam: Balkema.

Boulton, G. S., Dent, D. L., & Morris, E. M. (1974). Subglacial shearing and crushing, and the role of water pressures in tills from southeast Iceland. *Geografiska Annaler Series A*, *56*(3/4), 135–145.

Boulton, G. S., Dobbie, K. E., & Zatsepin, S. (2001). Sediment deformation beneath glaciers and its coupling to the subglacial hydraulic system. *Quaternary International*, *86*, 3–28.

Brown, N. E., Hallet, B., & Booth, D. B. (1987). Rapid soft bed sliding of the Puget glacial lobe. *Journal of Geophysical Research*, *92*(B9), 8985–8997.

Clark, C. D. (2010). Emergent drumlins and their clones: From till dilatancy to flow instabilities. *Journal of Glaciology*, *51*, 1011–1025.

Clark, C. D., Hughes, A. L. C., Greenwood, S. L., Spagnolo, M., & Ng, F. S. L. (2009). Size and shape characteristics of drumlins, derived from a large sample, and associated scaling laws. *Quaternary Science Reviews*, *28*, 677–692.

Clarke, G. K. C. (2005). Subglacial processes. *Annual Review of Earth and Planetary Sciences*, *33*, 247–276.

Clarke, G. K. C., Collins, S., & Thomson, D. (1984). Flow, thermal structure, and subglacial conditions of a surge-type glacier. *Canadian Journal of Earth Sciences*, *21*(2), 232–240.

Creyts, T. T., & Schoof, C. G. (2009). Drainage through subglacial water sheets. *Journal of Geophysical Research*, *114*, F04008. https://doi.org/10.1029/2008JF001215

Cuffey, K. M., & Paterson, W. S. B. (2010). *The physics of glaciers* (4th ed.). New York: Butterworth-Heinemann.

Damsgaard, A., Egholm, D. L., Piotrowski, J. A., Tulaczyk, S., Larsen, N. K., & Tylmann, K. (2013). Discrete element modelling of subglacial sediment deformation. *Journal of Geophysical Research: Earth Surface*, *118*, 2230–2242. https://doi.org/10.1002/2013JF002830

Ellwanger, D. (1992). Lithology and stratigraphy of some Rhine drumlins (South German Alpine Foreland). *Geomorphology*, *6*, 79–88.

Evans, D. J. A., & Hiemstra, J. F. (2005). Till deposition by glacier submarginal, incremental thickening. *Earth Surface Processes and Landforms*, *20*, 1633–1662.

Eyles, N., Putkinen, N., Sookhan, A., & Arbelaes-Moreno, L. (2016). Erosional origin of drumlins and megaridges. *Sedimentary Geology*, *338*, 2–23.

Fannon, J. S., Fowler, A. C., & Moyles, I. R. (2017). Numerical simulations of drumlin formation. *Proceedings of the Royal Society A*, *473*, 20170220.
Fowler, A. C. (2000). An instability mechanism for drumlin formation. In A. Maltman, M. J. Hambrey, & B. Hubbard (Eds.), *Deformation of subglacial materials* (Vol. 176, pp. 307–319). London, UK: Special Publication of the Geological Society.
Fowler, A. C. (2009). Instability modeling of drumlin formation incorporating lee-side cavity growth. *Proceedings of the Royal Society of London. Series A*, *465*, 2681–2702.
Fowler, A. C. (2010). The instability theory of drumlin formation applied to Newtonian viscous ice of finite depth. *Proceedings of the Royal Society of London. Series A*, *466*, 2673–2694.
Fowler, A. C., & Chapwanya, M. (2014). An instability theory for the formation of ribbed moraine, drumlins, and mega-scale glacial lineations. *Proceedings of the Royal Society A*, *470*, 20140185.
Goldstein, B. (1994). Drumlins of the Puget lowland, Washington state, USA. *Sedimentary Geology*, *91*, 299–311.
Gravenor, C. P. (1953). The origin of drumlins. *American Journal of Science*, *251*, 674–681.
Hindmarsh, R. C. A. (1998). Drumlinization and drumlin-forming instabilities: visCous till mechanisms. *Journal of Glaciology*, *44*, 293–314.
Hjartarson, Á. (2015). Heat flow in Iceland, *Proc. World Geotherm. Congress,* Melbourne, Australia, 19–25, April 2015.
Hooke, R. L. B. (2005). *Principles of glacier mechanics* (2nd ed.). New York: Cambridge University Press.
Hooke, R. L. B., & Medford, A. (2013). Are drumlins the product of a thermo-mechanical instability? *Quaternary Research*, *79*, 458–464.
Iverson, N. R. (2010). Shear resistance and continuity of till at glacier beds: Hydrology rules. *Journal of Glaciology*, *56*(200), 1104–1114.
Iverson, N. R., Hooyer, T. S., & Baker, R. W. (1998). Ring-shear studies of till deformation: Coulomb-plastic behavior and distributed strain in glacier beds. *Journal of Glaciology*, *44*(148), 634–642.
Iverson, N. R., Hooyer, T. S., Fischer, U. S., Cohen, D., Moore, P. L., Jackson, M., … Kohler, J. (2007). Soft-bed experiments beneath Engabreen, Norway: Regelation infiltration, basal slip, and bed deformation. *Journal of Glaciology*, *53*, 323–340.
Iverson, N. R., Hooyer, T. S., Thomason, J. F., Graesch, M., & Shumway, J. R. (2008). The experimental basis for interpreting particle and magnetic fabrics of sheared till. *Earth Surface Processes and Landforms*, *33*, 627–645.
Iverson, N. R., McCracken, R. G., Zoet, L. K., Benediktsson, Í. Ö., Schomacker, A., Johnson, M. D., … Everest, J. (2016). A theoretical model of drumlin formation based on observations at Múlajökull, Iceland. *Geophysical Research Abstracts, 18*, EGU2016–2655.
Iverson, N. R., & Semmens, D. J. (1995). Intrusion of ice into porous media by regelation: A mechanism of sediment entrainment by glaciers. *Journal of Geophysical Research*, *100*(B7), 10,219–10,230.
Iverson, R. M. (2003). How should mathematical models of geomorphic processes be judged? In P. R. Wilcock & R. M. Iverson (Eds.), *Prediction in geomorphology* (pp. 83–94). Washington, DC: American Geophysical Union.
Johnson, M. D., Schomacker, A., Benediktsson, Í. Ö., Geiger, A. J., Ferguson, A., & Ingólfsson, Ó. (2010). Active drumlin field revealed at the margin of Múlajökull, Iceland: A surge-type glacier. *Geology*, *38*, 943–946.
Jónsson, S. A., Schomacker, A., Benediktsson, Í. Ö., Ingólfsson, Ó., & Johnson, M. D. (2014). The drumlin field and the geomorphology of the Múlajökull surge-type glacier, central Iceland. *Geomorphology*, *207*, 213–220.
Kamb, B. (1991). Rheological nonlinearity and flow instability in the deforming bed mechanism of ice stream motion. *Journal of Geophysical Research*, *96*(B10), 16,585–16,595.
Kamb, B., Raymond, C. F., Harrison, W. D., Englehardt, H., Echelmeyer, K. A., Humphrey, N., … Pfeffer, T. (1985). Glacier surge mechanism: 1982–1983 surge of variegated glacier, Alaska. *Science*, *227*, 469–479.
Kamb, W. (1970). Sliding motion of glaciers: Theory and observation. *Reviews of Geophysics*, *8*(4), 673–728.
Lamsters, K., Karušs, J., Rečs, A., & Bērzinš, D. (2016). Detailed subglacial topography and drumlins at the marginal zone of Múlajökul outlet glacier, central Iceland: Evidence from low frequency GPR data. *Polar Science*, *10*, 470–475.
Larsen, N. K., Piotrowski, J. A., & Kronborg, C. (2004). A multiproxy study of a basal till: A time-transgressive accretion and deformation hypothesis. *Journal of Quaternary Science*, *19*, 9–21.
Lliboutry, L. (1979). Local friction laws for glaciers: A critical review and new openings. *Journal of Glaciology*, *23*(89), 67–95.
McCracken, R. G. (2015). Physical characteristics of drumlins, with implications for their formation at an active drumlin field, Múlajökull, Iceland (Master's thesis). Ames, Iowa: Iowa State University.
McCracken, R. G., Iverson, N. R., Benediktsson, Í. Ö., Schomacker, A., Zoet, L. K., Johnson, M. D., … Ingolfsson, Ó. (2016). Origin of the active drumlin field at Múlajökull, Iceland: New insights from till shear and consolidation patterns. *Quaternary Science Reviews*, *148*, 243–260.
Menzies, J. (1986). Inverse-graded units within till in drumlins near Caledonia, Southern Ontario. *Canadian Journal of Earth Sciences*, *23*, 774–786.
Menzies, J., Hess, D. P., Rice, J. M., Wagner, K. G., & Ravier, E. (2016). A case study in the New York Drumlin Field, an investigation using microsedimentology, resulting in the refinement of a theory of drumlin formation. *Sedimentary Geology*, *338*, 84–96.
Menzies, J. M. (1979). A review of the literature on the formation and location of Drumlins. *Earth-Science Reviews*, *13*, 315–349.
Minchew, B., Simons, M., Björnsson, H., Pálsson, F., Morlighem, M., Seroussi, H., … Hensley, S. (2016). Plastic bed beneath Hofsjökull Ice Cap, central Iceland, and the sensitivity of ice flow to surface meltwater flux. *Journal of Glaciology*. https://doi.org/10.1017/jog.2016.2
Mitchell, J. K. (1993). *Fundamentals of soil behavior* (2nd ed.). New York: John Wiley.
Möller, P., Dowling, T., Cleland, C., & Johnson, M. D. (2016). On the issue of equifinality in glacial geomorphology. *Geophysical Research Abstracts, 18*, EGU2016–13626.
Paola, C., & Voller, V. R. (2005). A generalized Exner equation for sediment mass balance. *Journal of Geophysical Research*, *110*, F04014. https://doi.org/10.1029/2004JF000274
Pedersen, V. K., & Egholm, D. L. (2013). Glaciations in response to climate variations preconditioned by evolving topography. *Nature*, *49*, 206–210.
Piotrowski, J. A. (1989). Relationship between drumlin length and width as a manifestation of the subglacial processes. *Zeitschrift für Geomorphologie N. F.*, *33*(4), 429–441.
Piotrowski, J. A., Larsen, N. K., & Junge, F. R. (2004). Reflections on soft subglacial beds as a mosaic of deforming and stable spots. *Quaternary Science Reviews*, *23*, 993–1000.
Rempel, A. W. (2008). A theory for ice–till interactions and sediment entrainment beneath glaciers. *Journal of Geophysical Research*, *113*, F01013. https://doi.org/10.1029/2007JF000870
Rempel, A. W. (2009). Effective stress and seepage flows beneath glacier and ice sheets. *Journal of Glaciology*, *55*(191), 431–443.
Rempel, A. W., Wettlaufer, J. S., & Worster, M. G. (2001). Interfacial premelting and the thermomolecular force: thermodynamic buoyancy. *Physical Review Letters*, *87*(8). https://doi.org/10.1103/PhysRevLett.87.088501
Schoof, C. (2007). Pressure-dependent viscosity and interfacial instability in coupled ice–sediment flow. *Journal of Fluid Mechanics*, *570*, 227–252.

Shaw, J. (2002). In defense of the meltwater (megaflood) hypothesis for the formation of subglacial bedform fields. *Journal of Quaternary Science*, *25*, 249–260.
Shreve, R. L. (1972). Movement of water in glaciers. *Journal of Glaciology*, *11*(62), 205–214.
Sigurkarlsson, M. F. (2015). Surge history of Múlajökull, Iceland, since 1945 detected with remote sensing data (Bachelor's thesis). Reykjavik: University of Iceland.
Stea, R. R., & Brown, Y. (1989). Variation in drumlin orientation, form, and stratigraphy relating to successive ice flows in southern and central Nova Scotia. *Geology*, *62*, 223–240.
Stokes, C. R., Fowler, A. C., Clark, C. D., Hindmarsh, R. C. A., & Spagnolo, M. (2013). The instability theory of drumlin formation and its explanation of their varied composition and internal structure. *Quaternary Science Reviews*, *62*, 77–96.
Stokes, C. R., Spagnolo, M., & Clark, C. D. (2011). The composition and internal structure of drumlins: Complexity, commonality, and implications for a unifying theory of their formation. *Earth-Science Reviews*, *107*, 398–422.
Tulaczyk, S. (1999). Ice sliding over weak, fine-grained tills: Dependence of ice–till interactions on till granulometry. *Geological Society of America Special Papers*, *337*, 159–177.
Tulaczyk, S., Kamb, B., & Engelhardt, H. (2000). Basal mechanics of Ice Stream B. I. Till mechanics. *Journal of Geophysical Research*, *105*, 463–481.
Turcotte, D. L., & Schubert, G. (2014). *Geodynamics* (3rd ed.). Cambridge, UK: Cambridge University Press.
Vreeland, N. P., Iverson, N. R., Graesch, M., & Hooyer, T. S. (2015). Magnetic fabrics of drumlins of the Green Bay Lobe, southeastern Wisconsin. *Quaternary Science Reviews*, *112*, 33–44.
Werder, M. A., Hewitt, I. J., Schoof, C. G., & Flowers, G. E. (2013). Modeling channelized and distributed subglacial drainage in two dimensions. *Journal of Geophysical Research: Earth Surface*, *118*, 2140–2158. https://doi.org/10.1002/jgrf.20146
Whittecar, G. R., & Mickelson, D. M. (1977). Sequence of till deposition and erosion in drumlins. *Boreas*, *6*, 213–217.
Woodard, J. (2017). Insights into drumlin development at Múlajökull, Iceland: A geophysical approach (Master's thesis). Madison, WI: University of Wisconsin.